MODELLING OF SPRAYS IN CONTAINMENT APPLICATIONS WITH A CMFD CODE

S. Mimouni [1] , J-S. Lamy [2], J. Lavieville,[1]

S. Guieu[3] , M. Martin[3]

stephane.mimouni@edf.fr,

(*(1) Electricité de France R&D Division, 6 Quai Watier F-78400 Chatou, France,*

(2) Electricité de France R&D Division, 1 av. du Général de Gaulle F-92140 Clamart, France,

(3) Electricité de France SEPTEN Division, 12-14 av. Dutriévoz, 69628 Villeurbanne, France

Abstract

During the course of a hypothetical severe accident in a Pressurized Water Reactor (PWR), spray systems are used in the containment in order to prevent overpressure in case of a steam break, and to enhance the gas mixing in case of the presence of hydrogen.
In the frame of the Severe Accident Research Network (SARNET) of the 6th EC Framework Programme, two tests was performed in the TOSQAN facility in order to study the spray behaviour under severe accident conditions: TOSQAN 101 and TOSQAN 113.
The TOSQAN facility is a closed cylindrical vessel. The inner spray system is located on the top of the enclosure on the vertical axis. For the TOSQAN 101 case, an initial pressurization in the vessel is performed with superheated steam up to 2.5 bar. Then, steam injection is stopped and spraying starts simultaneously at a given water temperature (around 25°C) and water mass flow-rate (around 30 g/s). The transient state of depressurization starts and continues until the equilibrium phase, which corresponds to the stabilization of the average temperature and pressure of the gaseous mixture inside the vessel.
The purpose of the TOSQAN 113 cold spray test is to study helium mixing due to spray activation without heat and mass transfers between gas and droplets.
We present in this paper the spray modelling implemented in NEPTUNE_CFD, a three dimensional multi-fluid code developed especially for nuclear reactor applications. An original model dedicated to the droplet evaporation at the wall is also detailed. Keeping in mind the Best Practice Guidelines[1], closure laws have been selected to ensure a grid-dependence as weak as possible.
For the TOSQAN 113 case, the time evolution of the helium volume fraction calculated shows that the physical approach described in the paper is able to reproduce the mixing of helium by the spray. But the transient behaviour should be improved by a better understanding of the influence of the dispersed phase on the turbulence of the continuous phase.
For the TOSQAN 101 case, droplet velocity, steam volume fraction and gas temperature profiles compare favourably with the experimental results. In the frame of the SARNET network, it seems that only the results obtained with the physical modelling implemented in the NEPTUNE_CFD code reproduces correctly the entrainment phenomena and the condensation zone (Malet, 2007).

1 NOMENCLATURE

A_i interfacial area concentration
C_d drag coefficient
d droplet diameter
dt numerical time step

[1] Best Practice Guidelines for the use of CFD in Nuclear Reactor Safety Applications, NEA/CSNI/R5 (2007)

$\underline{g}$ gravity acceleration
K_l liquid turbulent kinetic energy
$\underline{M_k}$ interfacial momentum transfer per unit volume and unit time
p pressure
Pr_k Prandtl number
t time
$\underline{u'_k}$ fluctuation of the velocity for the phase k
$\underline{V_k}$ averaged velocity of phase k
$\underline{V_{ki}}$ interfacial-averaged velocity
α_k denotes the volume fraction of phase k
ε_k dissipation rate
μ_k molecular viscosity
ν_k kinematic viscosity
ν_k^T turbulent eddy viscosity
ρ_k, averaged density of phase k

Subscripts/Superscripts
l liquid droplets
g gas
v vapour
a air
He Helium
k phase $k = 1$ or 2

2 INTRODUCTION

During the course of a hypothetical severe accident in a nuclear Pressurized Water Reactor (PWR), hydrogen may be produced by the reactor core oxidation and distributed into the reactor containment according to convective flows, water steam wall condensation and interaction with the spraying droplets. In order to assess the risk of detonation generated by a high local hydrogen concentration, hydrogen distribution in the containment vessel has to be known. The TOSQAN experimental programme has been created to simulate typical accidental thermal hydraulic flow conditions of the reactor containment. The aim of this work is thus to study the heat and mass exchanges between the spray droplets and the gas with thermal hydraulic conditions representative of this hypothetical severe accident.

To evaluate the spray modelling of containment codes, a benchmark was performed in the frame of the Severe Accident Research Network (SARNET) of the 6th EC Framework Programme. This benchmark was based on the TOSQAN experimental programme undertaken by the Institut de Radioprotection et de Sûreté Nucléaire (IRSN). The TOSQAN facility is a large enclosure devoted to simulate typical accidental thermal hydraulic flow conditions in nuclear-pressurized water reactor (PWR) containment. It is highly instrumented with non-intrusive optical diagnostics. Therefore, it is particularly adapted to nuclear safety CFD code validation.

Two tests were selected in order to evaluate separate effects involved when spray systems are used for containment applications. A first part, called the THERMALHYDRAULIC part, is relative to the thermodynamic of sprays, i.e. the droplet heat and mass transfer modelling and the gas thermodynamic modelling (TOSQAN 101 test). A second part, called the DYNAMIC part, is relative to the gas entrainment and atmosphere mixing induced by a spray, avoiding heat and mass transfer exchanges (TOSQAN 113 test).

Calculations have been done with 4 CFD codes namely GASFLOW, TONUS-CFD, CFX and NEPTUNE_CFD (Malet, 2006, 2007). For the two-phase flow with a gaseous mixture and spray droplets, the 3-dimensional code GASFLOW solves a homogeneous two-phase model (Kim, 2008). The spray effect in the commercial code CFX is taken into account by a lagrangian approach. The

TONUS-CFD code uses an eulerian model with a multi-component approach. The NEPTUNE_CFD spray modelling described in this paper is based on a two-fluid approach.

The paper is organized as follows. First we describe the set of equations solved in NEPTUNE_CFD. Next, turbulent terms and interfacial transfer terms are detailed. An original modelling of the wall transfer terms is proposed. In the last part, the two-phase flow model is validated by simulating the TOSQAN 113 and TOSQAN 101 tests on global and local variables.

3 THE NUMERICAL SOLVER AND PHYSICAL MODELING

3.1 Introduction

The solver, based on a pressure correction approach, is able to simulate multi-component multiphase flows by solving a set of three balance equations for each field (fluid component and/or phase) (Ishii, 1975), (Delhaye, 1981). These fields can represent many kinds of multiphase flows: distinct physical components (e.g. gas, liquid and solid particles); thermodynamic phases of the same component (e.g.: liquid water and its vapour); distinct physical components, some of which split into different groups (e.g.: water and several groups of different diameter bubbles); different forms of the same physical components (e.g.: a continuous liquid field, a dispersed liquid field, a continuous vapour field, a dispersed vapour field). The solver is implemented in the NEPTUNE software environment (Guelfi, 2007), (Mimouni, 2007, 2008), which is based on a finite volume discretization, together with a collocated arrangement for all variables. The data structure is totally face-based which allows the use of arbitrary shaped cells (tetraedra, hexaedra, prisms, pyramids ...) including non conforming meshes.

3.2 Governing equations and physical modelling

3.2.1 Main set of balance equations

The two-fluid model is constituted of the following six balance equations (Ishii, 1975):
Two mass balance equations:

$$\frac{\partial \alpha_k \rho_k}{\partial t} + \nabla.\left(\alpha_k \rho_k \underline{V}_k\right) = \Gamma_k \qquad k = 1,2 \tag{1}$$

with $\sum_k \alpha_k = 1$ *and* $\sum_k \Gamma_k = 0$,

where t is the time, α_k, ρ_k, $\underline{V}_k$ denote the void fraction of phase k, its averaged density and velocity and Γ_k is the interfacial mass transfer per unit volume and unit time. The phase index k takes the values *1* for the continuous phase (gas) and *2* for the dispersed phase (droplets).

Two momentum balance equations:

$$\frac{\partial \alpha_k \rho_k \underline{V}_k}{\partial t} + \nabla.\left(\alpha_k \rho_k \underline{V}_k \underline{V}_k\right) = -\alpha_k \underline{\nabla} p + \underline{I}_k + \alpha_k \rho_k \underline{g} + \nabla.\left[\alpha_k \left(\underline{\underline{\tau}}_k + \underline{\underline{\tau}}_k^T\right)\right] \qquad k = 1,2\,, \tag{2}$$

where p is the pressure, $\underline{g}$ is the gravity acceleration, $\underline{I}_k$ is the interfacial momentum transfer per unit volume and unit time, $\underline{\underline{\tau}}_k$ and $\underline{\underline{\tau}}_k^T$ denote the molecular and turbulent stress tensors (Reynolds stress tensor).

Two total enthalpy balance equations:

$$\frac{\partial}{\partial t}\left[\alpha_k \rho_k \left(h_k + \frac{V_k^2}{2}\right)\right] + \nabla.\left(\alpha_k \rho_k \left(h_k + \frac{V_k^2}{2}\right)\underline{V}_k\right) = \alpha_k \frac{\partial p}{\partial t} + \alpha_k \rho_k \underline{g}.\underline{V}_k + \Gamma_k \left(h_{ki} + \frac{V_k^2}{2}\right), \tag{3}$$
$$+ \Pi_k' A_i + \varphi_{wall \to k} - \nabla.\left[\alpha_k \left(\underline{q}_k + \underline{q}_k^T\right)\right] \qquad k = 1,2$$

where h_k is the phase-averaged enthalpy for phase k and h_{ki} is the interfacial-averaged enthalpy. We assumed that the two phases are governed by the same averaged pressure field p and we make no distinction between the pressures in the two phases or between the bulk pressure and the interface pressure for simplicity. The three terms Γ_k, (section 3.2.6) $\underline{I}_k$ (section 3.2.5) and $\Pi'_k A_i$ (section 3.2.6) denote the interfacial transfer terms of mass, momentum and heat, the quantity A_i being the interfacial area concentration.

The interfacial transfer of momentum $\underline{I}_k$ is assumed to be the sum of four forces:

$$\underline{I}_k = \Gamma_k \underline{V}_k + \underline{I}_k^D + \underline{I}_k^{AM} + \underline{I}_k^L . \tag{4}$$

The first term is the so-called *recoil* force that is the interfacial transfer of momentum associated to the interfacial transfer of mass, where we assumed the interfacial-averaged velocity $\underline{V}_{ki}$ to be equal to the phase-averaged velocity $\underline{V}_k$. The three other terms are the averaged drag, added mass and lift forces per unit volume. The lift and added mass force can be neglected in our calculations. The wall friction terms for the two phases do not appear in the momentum balance equations because solid walls are only present at the boundaries of the flow domain and the wall friction is expressed through the wall boundary conditions. The terms $\varphi_{wall\to k}$ denote the wall-to-fluid heat transfer per unit volume and unit time for each phase (section 3.2.7). The two terms $\underline{q}_k$ and $\underline{q}_k^T$ denote the molecular and turbulent heat fluxes inside phase k.

3.2.2 Equation of transport on the density of drops

If n is the density of drops, we define X_2 by $n = \alpha_2 \rho_2 X_2$ and write the following equation of transport of the density of drops:

$$\frac{\partial}{\partial t}(\alpha_2 \rho_2 X_2) + \nabla.(\alpha_2 \rho_2 X_2 \underline{V_2}) = K_{frag} - K_{coal} \tag{5}$$

with:

- K_{frag} the source term related to fragmentation.
- K_{coal} the source term related to coalescence.

In this paper, we neglect the fragmentation and coalescence phenomena (Alipchenkov, 2004). Therefore, the variations of the droplet diameter d are only due to the mass transfer between the droplets and the gaseous mixture (evaporation and condensation). Droplets are supposed to be of spherical shape:

$$\alpha_2 = n \cdot \frac{\pi . d^3}{6} \tag{6}$$

3.2.3 Mass balance equation of the non-condensable gas

$$\begin{cases} \frac{\partial}{\partial t}(\alpha_1 y_a \rho_1) + \nabla \cdot (\alpha_1 y_a \rho_1 \underline{V}_1) = 0 - \nabla \cdot (\alpha_1 y_a \rho_1 \underline{V}_{da}) \\ \frac{\partial}{\partial t}(\alpha_1 y_v \rho_1) + \nabla \cdot (\alpha_1 y_v \rho_1 \underline{V}_1) = \Gamma_{2\to 1} - \nabla \cdot (\alpha_1 y_v \rho_1 \underline{V}_{dv}) \\ \frac{\partial}{\partial t}(\alpha_1 \rho_1) + \nabla \cdot (\alpha_1 \rho_1 \underline{V}_1) = \Gamma_{2\to 1} - 0 \end{cases} \tag{7}$$

with $\underline{V}_{da}$ and $\underline{V}_{dv}$ the diffusion velocities of the air and vapour in the mixture respectively, given by Fick's law. The mass fraction of air and vapour are respectively y_a and y_v.

The 3rd equation is already solved and is the sum of the two previous ones. Therefore, for the sake of simplicity, we only solve the first equation.

If another non-condensable gas is added to the gaseous mixture like helium for the TOSQAN 113 test, we solve in addition the corresponding mass balance equation:

$\frac{\partial}{\partial t}(\alpha_1 y_{He}\rho_1) + \nabla\cdot(\alpha_1 y_{He}\rho_1 \underline{V}_1) = -\nabla.(\alpha_1 y_{He}\rho_1 \underline{V}_{dHe})$, where y_{He} is the mass fraction of helium.

3.2.4 Turbulent transfer terms

The Reynolds stress tensor for the continuous phase is modelled using the Boussinesq approximation:

$$\underline{\underline{\tau}}_1^T = \rho_1 \nu_1^T (\underline{\underline{\nabla}}\underline{V}_1 + \underline{\underline{\nabla}}^T \underline{V}_1) - \frac{2}{3}\underline{\underline{I}}(\rho_1 q_1^2 + \rho_1 \nu_1^T \nabla.\underline{V}_1), \quad (8)$$

where $\underline{\underline{I}}$ is the identity tensor, q_1^2 is the turbulent kinetic energy and ν_1^T is the liquid turbulent eddy viscosity for the continuous phase. The turbulent eddy viscosity is expressed by the following relation:

$$\nu_1^T = C_\mu \frac{(q_1^2)^2}{\varepsilon_1}, \quad (9)$$

where $C_\mu = 0.09$. The turbulent kinetic energy q_1^2 and its dissipation rate ε_l are calculated by using the two-equations K-ε approach. We take into account the turbulence of the dispersed phase by using an algebraic model, which leads to an algebraic closure for the turbulent energy of the drops $q_2^2 = \frac{1}{2} < u'_{2,i}\, u'_{2,i} >$ and the covariance gas-drops $q_{12} =< u'_{1,i}\, u'_{2,i} >$.

For the dispersed phase, the Reynolds stress tensor is closed using a Boussinesq-like hypothesis (Deutsch, 1992):

$$\underline{\underline{\tau}}_2^T = \rho_2 \nu_2^T (\underline{\underline{\nabla}}\underline{V}_2 + \underline{\underline{\nabla}}^T \underline{V}_2) - \frac{2}{3}\underline{\underline{I}}(\rho_2 q_2^2 + \rho_2 \nu_2^T \nabla.\underline{V}_2) \quad (10)$$

with :

- $\nu_2^T = \frac{1}{3} q_{12} \left(\tau_{12}^t - \frac{C_A^{12}\tau_{12}^F}{\frac{\rho_2}{\rho_1} + C_A^{12}} \frac{\tau_{12}^F}{2} \right) + \frac{1}{3} q_2^2 \tau_{12}^F$, the turbulent viscosity for the dispersed phase,
- $q_2^2 = q_1^2 \left(\frac{b^2 + \eta_r}{1 + \eta_r} \right)$, the gas turbulent kinetic energy,
- $q_{12} = 2q_1^2 \left(\frac{b + \eta_r}{1 + \eta_r} \right)$, the covariance of the dispersed phase,
- $b = \frac{1 + C_A^{12}}{\frac{\rho_2}{\rho_1} + C_A^{12}}$
- $\eta_r = \frac{\tau_{12}^t}{\tau_{12}^F}$, the ratio between the time scale of the continuous phase turbulence viewed by the dispersed phase (that takes into account crossing trajectories effect) and the characteristic time scale of the momentum transfer rate between the liquid and dispersed phases:

$$\tau_{12}^t = \frac{\tau_1^t}{\sigma_\alpha}\left(1 + C_\beta \xi_r^2\right)^{-\frac{1}{2}}$$

$$\tau_{12}^F = \frac{C_A^{12} + \rho_2}{F_D^{12}}$$

with σ_α is the turbulent Schmidt or Prandtl turbulent for the continuous phase, C_β is the crossing trajectories coefficient taken equal to 1.8, $C_A^{12} = \frac{\rho_2}{2\alpha_2}$ is the added mass coefficient.

- $\xi_r = \frac{< \left|V_r^{12}\right| >}{\sqrt{\frac{2}{3}K_1}}$ and $\tau_1^t = \frac{3}{2} C_\mu \frac{q_1^2}{\varepsilon_1}$.

$\underline{V}_r^{12} = \underline{V}_2 - \underline{V}_1 - \underline{V}_d$ is the local relative velocity between phases 1 and 2, expressed in terms of the total relative mean velocity and a drifting velocity due to the correlation between the instantaneous distribution of dispersed particles and the turbulent structure of the carrier fluid.
The drift velocity is given by:

$$V_d^{12} = -\frac{\tau_{12}^t q_{12}}{3} \frac{\nabla \alpha_2}{\alpha_1 \alpha_2}\ , \tag{11}$$

τ_{12}^t being the fluid-particle turbulent time scale given above.

3.2.5 Interfacial momentum transfer terms

The interfacial momentum between continuous and dispersed phases can be written as the sum of a laminar contribution and a turbulent contribution:

$$\underline{I}_k = \underline{I'}_k + \Gamma_k \underline{V}_k \text{ and } I'_{1\to 2} = I'^{lam}_{1\to 2} + I'^{turb}_{1\to 2}$$

with $I'^{lam}_{1\to 2} = -(\alpha_1 \alpha_2) F_D^{12} (V_2 - V_1)$. If we neglect the added mass force, the turbulent contribution can be simplified: $I'^{turb}_{1\to 2} = (\alpha_1 \alpha_2) F_D^{12} V_d^{12}$, (12)

where F_D^{12} is the drag coefficient between phases 1 and 2. ((Dufour, 2005) and (Alipchenkov *et al.* 2004)) and is expressed as:

$$F_D^{12} = \frac{\rho_2}{\alpha_1} \frac{1}{\tau_2^F} \text{ with } \frac{1}{\tau_2^F} = \frac{\rho_1}{\rho_2} \frac{3}{4} \frac{C_D}{d} < \left|V_r^{12}\right| >_2 \text{ and} \tag{13}$$

$$C_D = \begin{cases} \dfrac{24}{\mathrm{Re}_2}\left(1 + 0.15\,\mathrm{Re}_2^{0,687}\right) & if \quad \mathrm{Re}_2 = \dfrac{\rho_1 < \left|V_r^{12}\right| > d}{\mu_1} < 1000 \\ 0{,}445 & if \quad \mathrm{Re}_2 \geq 1000 \end{cases}$$

3.2.6 Interfacial mass transfer terms

If the mechanical terms are neglected in comparison to the thermal terms in the averaged form of the energy jump condition, this condition reduces to:

$$\sum_k \left(\Gamma_k h_{ki} + \Pi'_k A_i\right) \approx 0\ . \tag{14}$$

This relation (together with the mass jump condition $\Gamma_2 = -\Gamma_1$) allows to compute the mass transfer terms as a function of the interfacial heat transfer terms and the interfacial-averaged enthalpies h_{ki} :

$$\Gamma_1 = -\Gamma_2 = \frac{\Pi'_1 + \Pi'_2}{h_{2i} - h_{1i}} A_i\ , \tag{15}$$

where $h_{2i} - h_{1i}$ can be approximated by the latent heat.

The balance of heat and mass transfer between a drop and the gas mixture surrounding the drop leads to the expression of the mass transfer terms. Sometimes the gas density is missing in the formula found in the literature because in many applications the gas is essentially composed of air and then the density is about 1. Hence, it is worth providing some evidence of the necessity to include the gas density in the formula given in the following (Spalding, 1958), (Williams, 1953), (Faghri, 2006).

If we note G the mass flux and 's' the droplet surface, then $G_s.4\pi r_s^2$ is the mass flowrate on the surface of a drop, which is also equal to the mass flowrate of the evaporated liquid (there is no dissolution of gas in the drop): $G.4\pi r^2 = G_s.4\pi r_s^2$, where *r* is the distance to the centre of the droplet in spherical coordinates.

The conservation of the vapour gives $G_v.4\pi r^2 = G_{v,s}.4\pi r_s^2 = G_s.4\pi r_s^2$.

The vapour mass flowrate is split into two parts: a convective part and a diffusive part given by Fick's law: $G_v = G_v^{CV} + G_v^{Diff}$ thus $\left(y_v.G - \rho D.\frac{dy_v}{dr} \right).r^2 = G_s.r_s^2$.

The mass variation of a drop $\dot{m}$ is then given by:

$$\begin{cases} -\dot{m} = G_s.4\pi r_s^2 = 4\pi\rho_1.D.r_s.\ln(1+B_M) \\ B_M = \dfrac{y_{v,s} - y_{v,\infty}}{1 - y_{v,s}} \end{cases}$$

where B_M is the Spalding number of mass, and '∞' denotes a state far from the droplet in the gas.

Relative velocity between the drop and the gas increases the rate of mass transfer (evaporation-condensation). This effect can be taken into account using the Sherwood number defined by:

$$Sh = \frac{h_m.d}{D} = \frac{d}{D}.\frac{-\dot{m}}{4\pi r^2\left(\rho_{v,s} - \rho_{v,\infty}\right)} = \frac{-\dot{m}}{D.2\pi r.\left(\rho_{v,s} - \rho_{v,\infty}\right)}$$

Moreover, the correlations of Frössling/Ranz-Marshall are widely used:

$$\begin{cases} Sh = 2 + 0{,}56\,\mathrm{Re}^{1/2}\,Sc^{1/3} \\ Nu = 2 + 0{,}56\,\mathrm{Re}^{1/2}\,\mathrm{Pr}^{1/3} \end{cases} \quad (16)$$

The first correlation depends on the Schmidt number and the Reynolds number. Here we want to extend the relation obtained above for $\dot{m}$ if Re=0, i.e. Sh=2. That imposes the choice:

$-\dot{m} = 2\pi.Sh.\rho_1 D.r_s.\ln(1+B_M)$

We deduce the mass transfer in the core flow:

$$\Gamma_1^c = \frac{6\alpha_2}{d_2^2} Sh.D(T_m).\{\rho_1 \ln(1+B_M)\} \quad (17)$$

In the same way, the energy conservation combined with Fourier's law leads to:

$$\Gamma_1^c = \frac{6\alpha_2}{d_2^2} Nu.\frac{\lambda_1(T_m)}{c_{p1}(T_m)}.\{\ln(1+B_T)\} \quad (18)$$

with:

- $B_M = \dfrac{y_{sat}(T_2) - y_v}{1 - y_{sat}(T_2)}$ the number of Spalding of mass, the subscript 'sat' denoting the saturation state;
- $B_T = \dfrac{c_{p1}(T_m) \times (T_1 - T_2)}{-\dfrac{\Pi'_1}{\Gamma_1^c}}$ the number of Spalding of temperature;
- $y_v = \dfrac{\rho_v}{\rho_1}$ the vapour mass fraction in the gas mixture;

- *Sh* and *Nu* are respectively the Sherwood number and the Nusselt number;
- D the coefficient of diffusion of the vapour in the gas mixture;
- λ_1 the thermal conductivity of phase 1, c_{p1} the specific heat of the gas mixture;
- $T_m = \frac{2T_2 + T_1}{3}$ the film temperature, to which the physical quantities *D*, λ_1 and c_{p1} are estimated.

We can simplify the expressions of Γ_1^c and Π'_1. Indeed, if we consider the limit cases $B_M, B_T \to 0$ and $y_{sat}(T_2) \to 0$ the former expressions are simplified to obtain:

$$\begin{cases} \Gamma_1^c = \dfrac{6\alpha_2}{d_2^2} Sh.D(T_m).\{\rho_{sat}(T_2) - \rho_1 y_v\} \\ \Pi'_1 = \dfrac{6\alpha_2}{d_2^2} Nu.\lambda_1(T_m).\{T_2 - T_1\} \end{cases} \tag{19}$$

For the expressions of the Nusselt and Sherwood numbers, we use the correlations of Frössling/Ranz-Marshall (Ranz, 1952), with:

- $Sc = \frac{\mu_1}{\rho_1 D}$ the Schmidt number
- $\mathrm{Pr} = \frac{\mu_1 c_{p1}}{\lambda_1}$ the number of Prandtl
- $\mathrm{Re} = \frac{\rho_1 \left| V_r^{12} \right| d}{\mu_1}$ the Reynolds number
- $D(T) = 4{,}88.10^{-4} \times \frac{T\sqrt{T}}{P}$ the gas mixture diffusion coefficient (air/vapour).

3.2.7 Wall transfer model

We propose in this section an original model dedicated to the evaporation of droplets attached to a heated wall and surrounded by a hot gas.
The model of drop-wall interaction which was developed and implemented is written as a symmetric extension of the nucleate boiling model at the wall, and uses as a starting point the model of mass transfer in the core flow. To establish this original model, we made the following assumptions:

- the drops which accumulate on the walls take a hemispherical form;
- there is no nucleate boiling in the liquid film nor inside the drops at the wall;
- the drops which impact the walls successively see a stage of heating and a stage of evaporation;
- the droplets stick to the wall (no rebound).

The total heat flux exchanged between the wall and the flow is split into four terms:
• φ_{C1} a single-phase flow convective heat flux at the fraction of the wall area unaffected by the presence of droplets (heat transfer between the gas and the wall);
• φ_{C2} a single-phase flow convective heat flux at the fraction of the wall area affected by the presence of a liquid film (heat transfer between the liquid film and the wall);
• φ_{Th} a single-phase flow heat flux to increase the droplet temperature and reach the saturation state (heat transfer between the droplets and the wall);
• φ_E a vaporisation heat flux.

$$\varphi_{wall} = \varphi_{wall\to 1} + \varphi_{wall\to 2} \text{ with } \begin{cases} \varphi_{wall\to 1} = f_{\alpha_1}\varphi_{C_1} + \Gamma_w^{evap} h_{1i} \\ \varphi_{wall\to 2} = f_{\alpha_1}\varphi_{Th} - \Gamma_w^{evap} h_{2i} + (1 - f_{\alpha_1})\varphi_{C_2} \end{cases} \quad (20)$$

A classical law of single phase flow heat transfer at the wall is used to predict the flux:

$\varphi_{C_1} = (1 - A_g) h_{\log}^{vap} (T_w - T_\delta)$ and $\varphi_{C_2} = h_{\log}^{liq} (T_w - T_2)$ (21)

T_δ is the temperature of a point located in the turbulent boundary layer of the gas mixture, $h_{\log}^{vap}$ and $h_{\log}^{liq}$ are respectively the coefficients of heat transfer within the thermal boundary layers of the gas mixture and the film liquid phase. A_g is the sum of the areas of influence of each droplet over the unit surface.

$\Gamma_w^{evap} = \Gamma_{w\to 1} = -\Gamma_{w\to 2}$ represents the interfacial mass transfer at the wall caused by the droplets evaporation : $f_{\alpha_1} \cdot \varphi_E = \Gamma_w^{evap} (h_{1i} - h_{2i})$ (22)

f_{α_1} is a phenomenological function introduced to take into account the case where the dispersed phase becomes continuous near the wall : drops accumulate on the wall and form a liquid film.

The choice implemented in the code is as follows:

$$f_{\alpha_1} = \begin{cases} 1 - \dfrac{\exp[-20(\alpha_1 - \alpha_{crit})]}{2} & if \quad \alpha_1 > \alpha_{crit} \\ \dfrac{1}{2}\left(\dfrac{\alpha_1}{\alpha_{crit}}\right)^{20\alpha_{crit}} & if \quad \alpha_1 \le \alpha_{crit} \end{cases} \quad \text{and } \alpha_{crit} = 0.2 \quad (23)$$

We can now rewrite the total flow of energy yielded by the wall to the two phases in the following way: $\varphi_{wall} = f_{\alpha_1}\left(\varphi_{C_1} + \dfrac{\tau_c}{\tau_{tot}}\tilde{\varphi}_{Th} + \varphi_E\right) + (1 - f_{\alpha_1})\varphi_{C_2}$. (24)

Our model must still provide the expressions of $\tilde{\varphi}_{Th}$, A_g, $\dfrac{\tau_c}{\tau_{tot}}$ and Γ_w^{evap} .

3.2.7.1 Modelling of Γ_w^{evap}

As we suppose that the drops at wall are hemispherical with a diameter d_w , the volume conservation leads to: $d_w = 2r_w = 2^{1/3} d$. (25)

For the calculation of the heat and mass transfers at the wall, we suppose that the drops located at the wall are sufficiently distant the one from the others, and we neglect the side effects.

Heat is conducted through the droplet to the interface, where an abrupt temperature drop takes place due to evaporation. The mass fraction of the vapour component in the gas mixture is maximum at the interface, and by diffusion the mass fraction decreases to its bulk level with increasing distance from the wall. As time goes by, the liquid droplet becomes smaller, while the temperature at the heated wall and interface remains unchanged. Therefore, the mass transfer for a droplet can be expressed as:

$\dot{m}_d = \pi . Sh . D(T_m) . r_w (\rho_{sat}(T_w) - \rho_1 . y_v)$ (26)

and so : $\tilde{\Gamma}_w^{evap} = n_w \cdot \dot{q}_m = n_w \cdot \pi . Sh . D(T_m) . r_w (\rho_{sat}(T_w) - \rho_1 . y_v)$ (27)

with n_w the surface density of drops on the wall. We neglect the droplets velocity at the wall, which gives $Sh = 2$.

Finally: $\widetilde{\Gamma}_w^{evap}\dfrac{\tau_v}{\tau_{tot}}=\Gamma_w^{evap}$ and our model must still provide the expression of $\dfrac{\tau_v}{\tau_{tot}}$.

3.2.7.2 Modelling of $\widetilde{\varphi}_{Th}$

A simple approximate analysis is done below by estimating the conduction in the liquid droplet by the following correlation:

$$\dot{q}_{Th}=\lambda_2\overline{A}\frac{T_w-T_2}{\overline{\delta}}$$

where $\overline{A}$ and $\overline{\delta}$ are the average cross-sectional area of heat conduction and the average path length of the conduction, respectively. For a hemispherical droplet, the contact area between the droplet and the heated wall is πr_w^2 and the interfacial area of the droplet is $2\pi r_w^2$. Thus, we can take the average conduction area as:

$$\overline{A}=\frac{1}{2}\left(\pi r_w^2+2\pi r_w^2\right)=\frac{3}{2}\pi r_w^2$$

The average path length for conduction is:

$$\overline{\delta}=\frac{V}{\overline{A}}=\frac{(2/3)\pi r_w^3}{(3/2)\pi r_w^2}=\frac{4}{9}r_w$$

Therefore, the conduction in the liquid droplet becomes: $\dot{q}_{Th}=\dfrac{27}{8}\pi\lambda_2 r_w\left(T_w-T_2\right)$ (28)

We then deduce the following expression: $\widetilde{\varphi}_{Th}=n_w\ \dot{q}_{Th}$. (29)

3.2.7.3 Modelling of the density of drops at wall

The calculations of $\widetilde{\Gamma}_w^{evap}$ and $\widetilde{\varphi}_{Th}$ use the density of drops at wall. It is a problem which cannot be properly solved in a eulerian approach, which does not allow differentiating the drops at wall from the others. The number of droplets in the nearest cell to the wall is $N_2=\alpha_2\rho_2X_2S_{cell}h_{cell}$ where $S_{cell}h_{cell}$ is the volume of the cell with S_{cell} the surface projected onto the wall. We can suppose that droplets at a distance lower than d are sprayed onto the wall. Thus, we are only interested in the number of droplets in the volume $d\ S_{cell}$. The number of droplets at the wall by surface unit is obtained by dividing by S_{cell} :

$n_w=Min\left(n\ d,n_{\max}\right)$ with $n_{\max}=\dfrac{1}{\pi r_w^2}$. (30)

It is important to note that the result does not depend on the mesh.

The wall surface unit is split into two parts : an area influenced by droplets A_g and a "single phase area" A_c with the relation $A_g+A_c=1$. A_g is the sum of the areas of influence of each droplet over the unit surface. Neglecting the overlapping areas of influence between adjacent droplets, A_g is written :

$A_g=Min\left(1,n_w\pi r_w^2\right)$, (31)

and finally : $\varphi_{C_1}=(1-A_g)h_{\log}^{vap}\left(T_w-T_\delta\right)$. (32)

3.2.7.4 Modelling of the heating and evaporation time scale

The evaporation of the droplets sprayed onto the hot surface is split into two stages:

- a stage of heating described by the heat flux $\widetilde{\varphi}_{Th} = n_w \cdot \frac{27}{8}\pi\lambda_2 r_w (T_w - T_2)$ during the time τ_c and the energy providing by the wall to a droplet is $Q_c = \dot{q}_{Th} \cdot \tau_c$;

- a stage of evaporation described by $\widetilde{\Gamma}_w^{evap} = n_w \cdot \pi.Sh.D(T_m).r_w(\rho_{sat}(T_w) - \rho_1.y_v)$ during the time τ_v and the energy providing by the wall to a droplet is $Q_v = \dot{q}_m \cdot \tau_v \cdot L_{vap}$.

The total average flux provided by the wall to a droplet can be expressed by:

$$\phi_{tot} = \frac{Q_c + Q_v}{\tau_c + \tau_v} = \frac{\tau_c}{\tau_{tot}}\dot{q}_{Th} + \frac{\tau_v}{\tau_{tot}}\dot{q}_m L_{vap} \tag{33}$$

Finally, we obtain the following formula:

$$\varphi_{Th} = \frac{\tau_c}{\tau_{tot}}\widetilde{\varphi}_{Th} = n_w \cdot \frac{\tau_c}{\tau_{tot}}\frac{27}{8}\pi\lambda_2 r_w (T_w - T_2) \tag{34}$$

$$\text{and } \Gamma_w^{evap} = n_w \frac{\tau_v}{\tau_{tot}}\pi.D(T_m).Sh.\, r_w(\rho_{sat}(T_w) - \rho_1.y_v) \tag{35}$$

It remains to determine the heating and evaporation time scale τ_c and τ_v. The heating time scale is obtained by solving a simplified heat conduction equation for a hemispherical droplet heated by a hot wall. The liquid droplet is initially at the temperature $T = T_2$ and heated via the term of conduction $\dot{q}_{Th}$:

$$\rho_2 c_{p2}\frac{4}{3}\pi r_w^3\frac{\partial T}{\partial t} = \frac{27}{8}\pi\lambda_2 r_w (T_w - T)$$

and by scale analysis: $\tau_c = 2\left(\frac{2}{3}\right)^4 \frac{r_w^2}{a_2}$ where $a_2 = \lambda_2 / \rho_2 c_{p2}$. (36)

The energy balance at the interface of a hemispherical droplet at the temperature T_w can be written as:

$$\rho_2 L_{vap} 2\pi r_w^2 \frac{dr_w}{dt} = L_{vap}\dot{q}_m = L_{vap}\pi.D(T_m).Sh.r_w(\rho_{sat}(T_w) - \rho_1.y_v)$$

and after integration: $\tau_v = \frac{\rho_2 r_w^2}{Sh.D.(\rho_{sat}(T_w) - \rho_1.y_v)}$ (37)

4 TOSQAN FACILITY

The TOSQAN facility and the associated measurement levels are presented in (Lemaitre, 2005), (Malet, 2005, 2006, 2007) and illustrated in Figure 1. It is a closed cylindrical vessel (7 m^3 volume, 4.8 m high, 1.5 m internal diameter). The vessel walls are thermostatically controlled by heated oil circulation. The inner spray system is located on the top of the enclosure on the vertical axis. It is composed of a single nozzle producing a full-cone water spray. In the lower part of the vessel, the water impacting the sump is removed to avoid water accumulation and to limit evaporation.

Gas temperature, volume fractions and droplets velocity measurements are available on TOSQAN at different heights *Z*.

4.1 TOSQAN Test 113 sequence

The TOSQAN spray Test 113 focuses on the dynamical effects of spray systems on entrainment and mixing of gases avoiding important heat and mass transfer exchanges.

The gas mixture is initially stratified: helium in the upper part of the vessel, and air in the lower part of the vessel. When the spray is activated, gas mixture is entrained, generating a global flow that leads to a global mixing in the vessel after several hundreds seconds.
The initial helium stratification is given in Table 1. Symmetry has been checked experimentally so that the given values can be used on the whole radius. The main spray characteristics are given in Table 2.

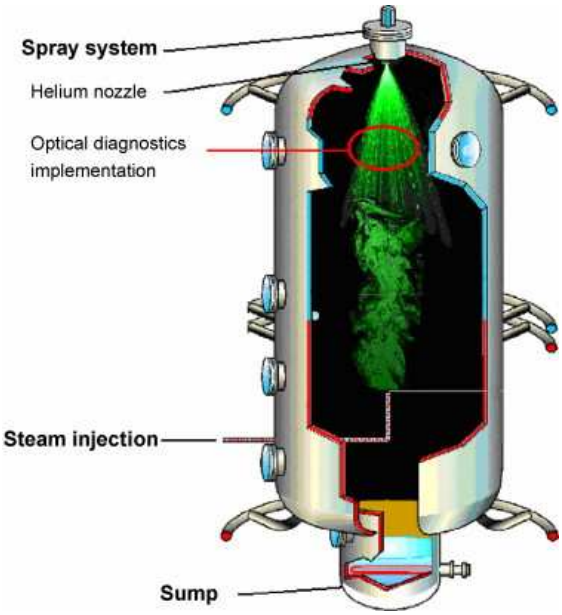

Figure 1:TOSQAN facility


Figure 2:Meshing used for the TOSQAN calculations

Table 1: Experimental gas initial conditions before spray injection (t = 0 s) in TOSQAN 113.

Z (from the bottom)	**Helium concentration (%)**	**Mean gas temperature (°C)**
Z13 = 3.93 m	99.0 +/- 0.5	31.8
Z11 = 3.135 m	85.8 +/- 0.5	36.9
Z10 = 2.8 m	47.6 +/- 1.0	At Z9 = 2.675 m : 34.72
Z5 = 1.9 m	2.3 +/- 0.5	At Z6 = 2.045 m : 30.13
Z1 = 0.87 m	1.9 +/- 0.5	At Z2 = 1.21 m : 28.7

Table 2: Experimental spray characteristics in TOSQAN 113.

Spray flow-rate	30 g/s
Spray angle	55°C
Spray injection height	0.65 m from the top on TOSQAN axis
Initial droplet initial size	200 μm in the calculations
Initial droplet velocity	Around 10 m/s
Droplet injection temperature (°C)	30°C

The flow is assumed to be axisymmetric so that a two-dimensional axisymmetric mesh is used. Computations have been performed on two kinds of meshing : a grid with 4460 cells (Figure 2) and a fine grid with 40140 cells. Results are similar (Figure 6) between “standard” (4460 cells) and fine mesh (40140 cells). Hence, the subsequent computations are performed on the first grid.
According to (Malet, 2007), helium stratification break-up by spray in TOSQAN Test 113 can be divided into 3 stages: direct entrainment by the spray (Figure 3), global mixing by the spray (Figure 5), slow diffusive mixing of the helium in the dome.
The time evolution of the helium volume fraction measured by two sensors located respectively near the top and near the bottom of the TOSQAN vessel is represented on Figure 4. A reasonable agreement is obtained between experimental data and code calculation but the mixing time occurs slightly too fast in the simulation.

Some calculations have been performed to test the sensitivity to the turbulence model for both dispersed and continuous phase (not presented in the paper). Eddy Viscous Model and Reynolds Stress Transport Model applied to the continuous phase give similar results. Tests performed on the turbulence model of the dispersed phase give also similar results. A better understanding of the spray effects is still needed.

The sensitivity to the droplet diameter (150, 200 ("standard"), 250 and 500 μm) is weak (Figure 6).

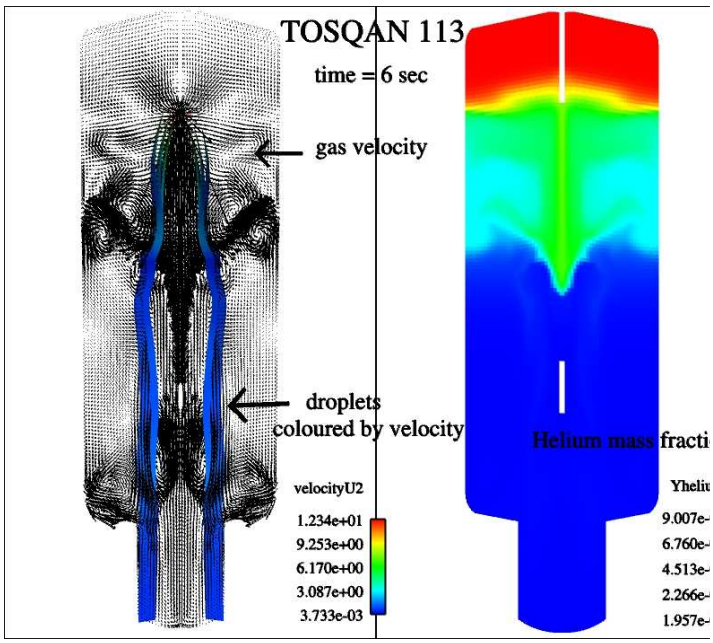

Figure 3:Gas velocity, droplet velocity and helium mass fraction at t=6 sec.

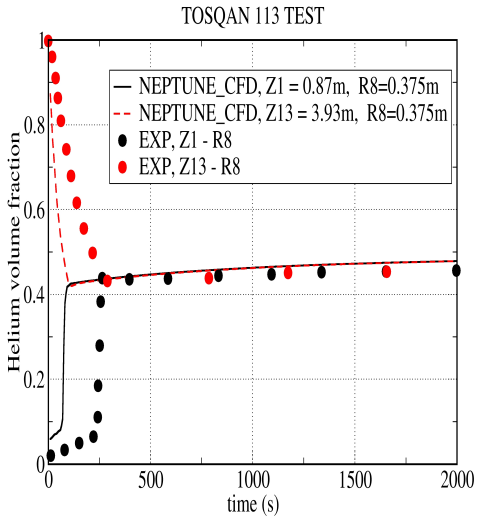

Figure 4: Time evolution of the helium volume fraction measured by two sensors located respectively near the top and near the bottom of the TOSQAN vessel.

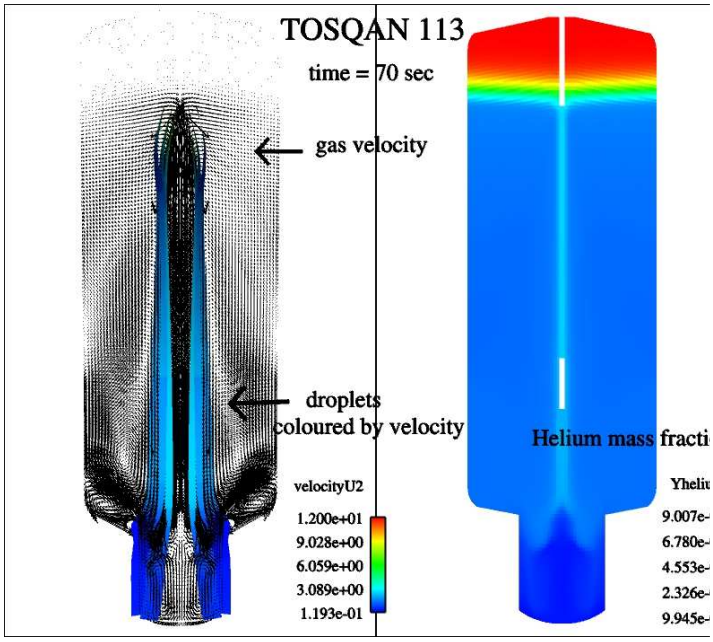

Figure 5:Gas velocity, droplet velocity and helium mass fraction at t=70 sec.

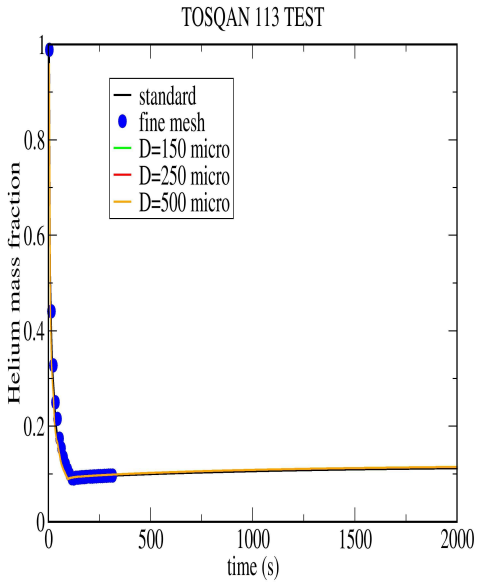

Figure 6: Time evolution of the helium mass fraction measured by a sensor located near the top of the TOSQAN vessel. : sensitivity to the

mesh refinement and to the droplet diameter.

4.2 TOSQAN test sequence 101

The night before test 101, compressed air is injected into the open TOSQAN vessel in order to remove steam from former tests. On the morning of the spray test, the air injection is stopped. When a thermal steady state is reached, the vessel is closed (the vessel relative pressure is then 0 bar).

An initial pressurization in the vessel is performed with superheated steam up to 2.5 bar. Then, steam injection is stopped and spraying starts simultaneously at a given water temperature (around 25°C) and water mass flow-rate (around 30 g/s).

The transient state of depressurisation starts and continues until the equilibrium phase, which corresponds to the stabilization of the average temperature and pressure of the gaseous mixture inside the vessel.

The test conditions are given in Table 3 for the gas initial conditions and

Table 4 for the spray characteristics during the test. The mean wall temperature is about 120°C.

Table 3: Experimental gas initial conditions before spray injection (t = 0 s) in TOSQAN 101.

Mean gas temperature out of the spray zone	131.1°C
Mean gas temperature in the spray zone	131.0°C
Total pressure	2.5 bar
Initial gas composition (from mass balance)	213 moles of air + 308 moles of steam, (59.1%vol steam)

Table 4: Experimental spray characteristics in TOSQAN 101.

Spray flow-rate	29.96 g/s
Spray angle	55°
Water injection temperature (°C) At t=0 s At t=311 s At t=1000 s	Mean value integrated over 5 s at the given time – linear interpolation between two steps 119.1°C 22.1°C 27.7°C
Nozzle position	65 cm (Z14bis) from the top on the TOSQAN axis (R12)
Droplet velocity 5 cm below the nozzle	10 m/s flat profile
Spray half-width 5 cm below the nozzle	27.1 mm
Droplet size	D_{10} =200 µm

The wall temperature is maintained constant at 120 °C during the whole test. The atmosphere in the vessel is an air–steam mixture with a relative humidity of 75%, in which the mixture is assumed to be initially homogeneous with a pressure of 2.5 bars. We will see below that the mixture is not really initially homogeneous: the initial conditions for calculations are not fully representative of the experimental conditions.

Figure 7 and Figure 8 illustrate respectively the temperature of the air-steam mixture and the air mass fraction at the end of the steam injection. Calculations show that both fields of temperature and mass fraction are not homogeneous. If the spray starts from this state, droplets enter in a dry and hot zone which leads to a fast vaporization during about 100s. The direct entrainment by the spray is the main dynamical phenomenon during this stage. After this first stage, we observe a global mixing by the spray and the mixture can be assumed to be homogeneous.

But, for the benchmark, the mixture is assumed to be initially homogeneous with a pressure of 2.5 bar.

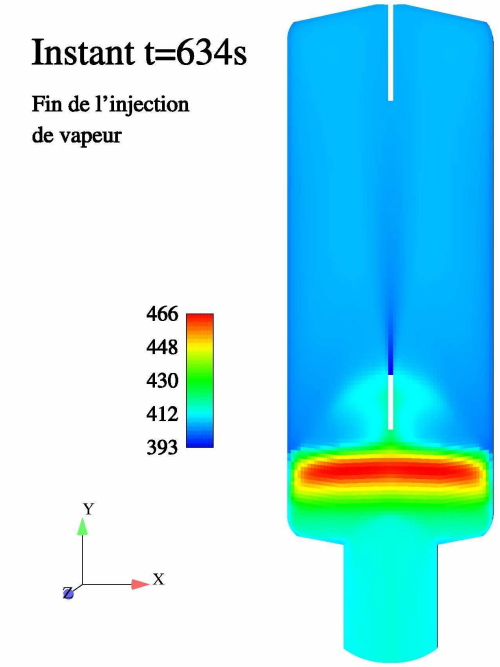

Figure 7: Temperature (K) of the air-steam mixture at the end of the steam injection.

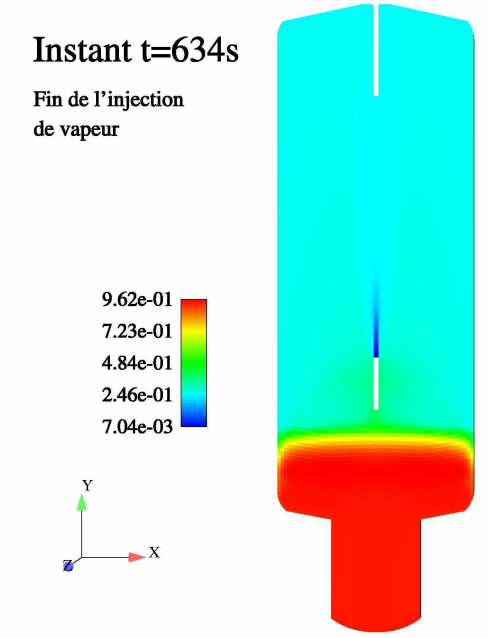

Figure 8: Air mass fraction at the end of the steam injection.

The experimental results (Porcheron, 2007) show that four phases can be observed:

- Phase A : Vaporization phase (strong increase of gas moles number; strong decrease of gas temperature);
- Phase B : Fast condensation phase up to gas saturation (Strong condensation, gas moles number decrease, gas cooling due to convective heat transfer between gas and droplets);
- Phase C : Saturated gas, slow condensation phase up to thermodynamic equilibrium (Gas cooling due to convective heat transfer between gas and droplets);
- Phase D : Thermodynamic equilibrium (Equilibrium between heat taken by droplets and heat given by wall).

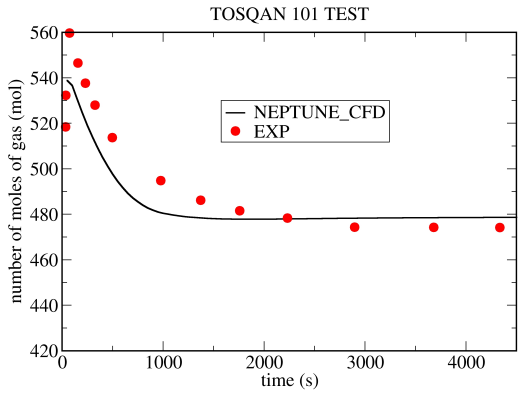

Figure 9: Time evolution of the number of moles of gas

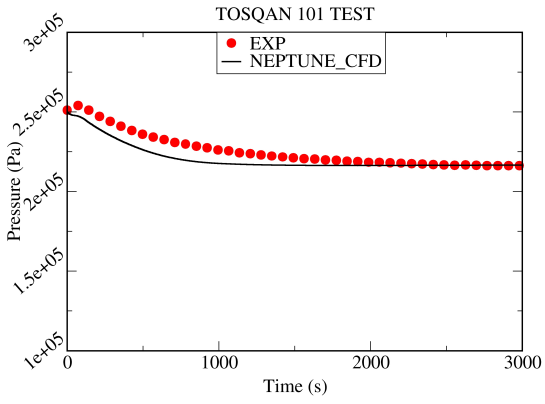

Figure 10: Time evolution of the pressure

Results obtained for the pressure time evolution are presented on Figure 10. The gas mole number time evolution is presented on Figure 9. It can be seen that the numerical results obtained for these global variables are in good agreement with the experimental data for the steady-state levels. If we don't take into account the evaporation of the droplets at the wall, then the pressure equilibrium tends to 1 bar.

Concerning the transient phase, more discrepancies are obtained: calculations underestimate the pressure during the transient phase.
However, the main objective of this TOSQAN benchmark was to recover the final steady-state, so that the boundary conditions of the first instants during the tests were not detailed specifically. As a result, numerical data cannot recover exactly the experimental ones during the initial period of the transient phases. Moreover, not enough measurements during this transient phase are available to compute the detailed phase A.
The same kind of considerations can be done for the gas mole number time evolution: the steady state is quite well reproduced but the transient phase leads to higher discrepancies.

The droplet vertical velocity on the Z14 horizontal axis (4 m) is presented on Figure 15. Results are in a reasonable agreement with the experimental data. Calculations present a large spray width because of the entrainment caused by the droplets. The spray width is in good agreement and so the modelling of the entrainment caused by the droplets seems quite realistic.
Calculations show a recirculation loop with positive velocities near the walls indicating one big flow loop in the vessel. This result is made possible only if the relative velocity is different from zero which is the case with the two-fluid approach considered here since we solve momentum equations for both the liquid and the gas phase.
Moreover, calculations show an almost linear deceleration of the gas and droplet velocities, without equilibrium velocity.

Following Mallet et al. (Mallet, 2007), it should be also emphasized that results provided by calculations for the droplet temperature are quite realistic (Figure 16). Even if no droplet temperature has been measured for this test, measurements of droplet temperature exist for a similar test but with an off-centred spray nozzle (test A1, see (Malet, 2007)). Results show that the droplet temperature increase is located in the first 15 cm close to the spray nozzle. Even if this value can change from test A1 to test 101 (mainly because of a higher influence of the wall temperature on the spray region in test A1, resulting in a higher gas temperature on spray axis), the distance on which the droplet temperature has reached a constant value should not change drastically.

Steam volume fraction (SVF) radial profiles are presented on Figure 12 and Figure 14. Calculations show a lower value of the SVF out of the spray region (around 53%vol, i.e. 0.06 bar lower than the mean value assuming homogeneous field) and a greater value in the spray region. Therefore vapour condenses on the surface of the droplets in the spray region and then the gas temperature decreases (Figure 11 and Figure 13). As a result, the droplets temperature increases in the spray region along the vertical axis (Figure 16).

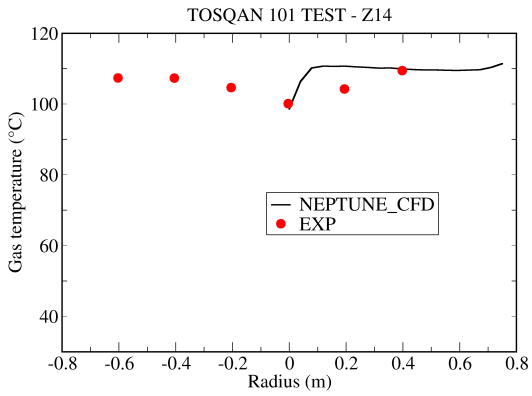

Figure 11: Radial profile of the gas temperature, on the Z14 horizontal axis, at equilibrium.

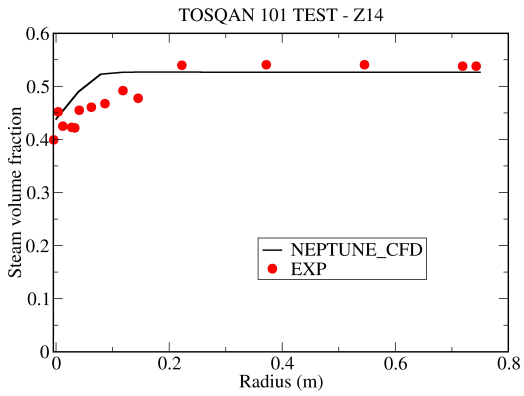

Figure 12: Radial profile of the steam volume fraction, on the Z14 horizontal axis, at equilibrium.

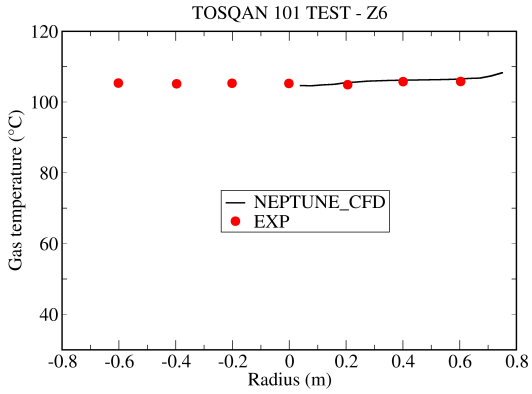

Figure 13: Radial profile of the gas temperature, on the Z6 horizontal axis (2.045 m), at equilibrium.

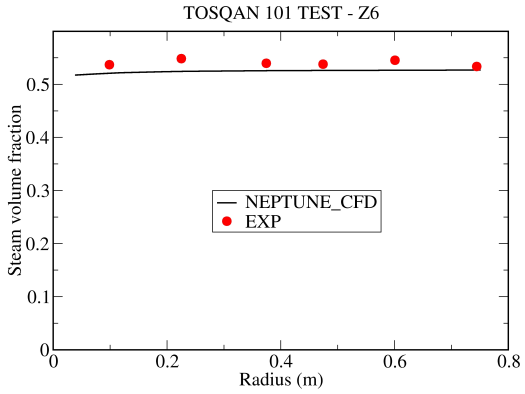

Figure 14: Radial profile of the steam volume fraction, on the Z6 horizontal axis (2.045 m), at equilibrium.

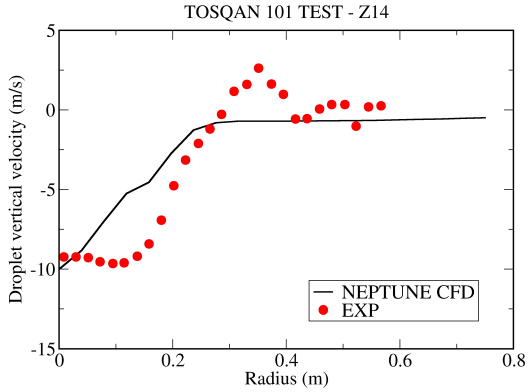

Figure 15: Radial profile of the droplet vertical velocity, on the Z14 horizontal axis (4 m), at equilibrium.

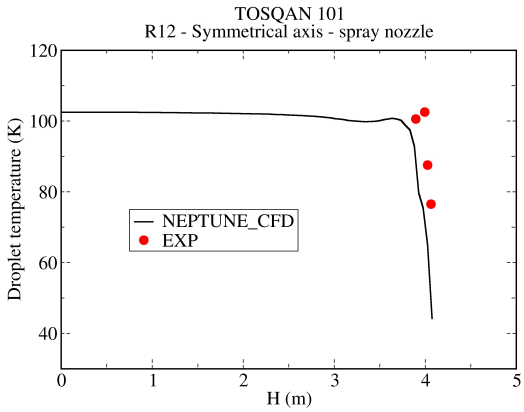

Figure 16: Axial profile of the droplet temperature along the symmetrical axis (R12).

5 CONCLUSION

We have presented in this paper the spray modelling implemented in NEPTUNE_CFD, a three dimensional two-fluid code dedicated to nuclear reactor applications. This local three-dimensional solver is based on the classical two-fluid one pressure approach, including mass, momentum and energy balances for each phase. Thanks to a code–to-experiment benchmark based on 2 tests of the TOSQAN facility, we successfully evaluated the ability of the code to reproduce the droplet heat and mass transfer on the one hand (TOSQAN 101 case) and the gas entrainment and atmosphere mixing by the spray on the other hand (TOSQAN 113 case). An original model dedicated to the droplet evaporation at the wall is also proposed.

During the course of a severe accident in a Pressurized Water Reactor (PWR), spray systems are used in a containment the size of which is much larger than the TOSQAN vessel studied in this paper. Therefore, it seems that the diameter variations of the droplets caused by collision, fragmentation and coalescence should be taken into account in future calculations.

6 ACKNOWLEDGMENTS

This work has been achieved in the framework of the PAGODES2 project financially supported by EDF (Electricité de France). The NEPTUNE_CFD code is being developed in the framework of the NEPTUNE project financially supported by CEA (Commissariat à l'Energie Atomique), EDF (Electricité de France), IRSN (Institut de Radioprotection et de Sûreté Nucléaire) and AREVA-NP.

7 REFERENCES

Alipchenkov, Nigmatulin, Soloviev, Stonik, Zaichik, Zeigarnik (2004), "A three-fluid model of two-phase dispersed annular flow", *International Journal of Heat and Mass Transfer* 47 (2004) 5323-5338.

J-M. Delhaye, M. Giot and M.L. Riethmuller, *Thermal-hydraulics of two-phase systems for industrial design and nuclear engineering*,. Hemisphere and McGraw Hill, 1981.

E. Deutsch, « Dispersion de particules dans une turbulence homogène isotrope stationaire calculée par simulation numérique directe des grandes échelles », *PhD Thesis IMFT*, in French, 1992.

G. Dufour, « Modélisation multi-fluide eulérienne pour les écoulements diphasiques à inclusions dispersées », *PhD Thesis*, Université Paul Sabatier, Toulouse III, in French, 2005.

A. Faghri, Y. Zhang, *Transport Phenomena in Multiphase Systems*, Elsevier, 2007.

A. Guelfi, D. Bestion, M. Boucker, P. Boudier, P. Fillion, M. Grandotto, J-M. Hérard, E. Hervieu, P. Péturaud, "NEPTUNE - A new software platform for advanced nuclear thermal hydraulics", *Nuclear Science and Engineering*, vol. 156, pp. 281-324, 2007.

M. Ishii, *Thermo-fluid dynamic, theory of two phase*, Eyrolles, collection de la direction des Etudes et recherches d'Electricité de France, 1975.

K. Jongtae, L. Unjang, W.H. Seong, K. Sang-Baik, K. Hee-Dong, "Spray effect on the behavior of hydrogen during severe accidents by a loss-of-coolant in the APR1400 containment", *International Communications in Heat and Mass Transfer* 33 (2006) 1207–1216.

P. Lemaitre, A. Nuboer, E. Porcheron, « TOSQAN Experimental Programme, Spray test n°101 », *technical report*, DSU / SERAC / LECEV / 05-11 (IRSN 91192 Gif sur Yvette, France), 2005.

J Malet, F. Dumay, E. Porcheron, P. Lemaitre, J. Vendel J., « TOSQAN Spray Benchmark n°1, TOSQAN Test 101 : Spray activation in air-steam mixture, Code-experiment comparison report », *technical report,* DSU / SERAC / LEMAC / 05-07 (IRSN 91192 Gif sur Yvette), 2005.

J. Malet, P. Lemaitre, E. Porcheron, J. Vendel, A. Bentaib, W. Plumecocq, F. Dumay, Y.-C., Chin, M. Krause, L. Blumenfled, F. Dabbene, P. Royl, J. Travis, "Modelling of Sprays in Containment Applications: Results of the TOSQAN Spray Benchmark (Test 101)", workshop ERMSARP 2006.

J. Malet, P. Métier, "SARNET SPRAY BENCHMARK THERMALHYDRAULIC part TOSQAN test 101 Code-experiment comparison report", *technical report*, DSU/SERAC/LEMAC/07-03 December 2007.

S. Mimouni, A. Archer, J. Laviéville, M. Boucker, N. Méchitoua, « Modeling and computation of unsteady cavitation flows", *La Houille Blanche*, N°6, 2006.

S. Mimouni, M. Boucker, J. Laviéville, A. Guelfi, D. Bestion, "Modeling and computation of cavitation and boiling bubbly flows with the NEPTUNE_CFD code", *Nucl. Eng. And Design* 238 (2008) pp 680-692.

E. Porcheron, P. Lemaitre, A. Nuboer, V. Rochas, J. Vendel, "Experimental investigation in the TOSQAN facility of heat and mass transfers in a spray for containment application", *Nuclear Engineering and Design*, Volume 237, Issues 15-17, September 2007, Pages 1862-1871

W.E. Ranz, W.R. Marschall, "Evaporation from drops", *Chem. Eng. Prog*., 48, pp. 173-180, 1952.

D.B. Spalding, "The combustion of liquid fuels", *Proceedings of the 4th Symp. (International) on Combustion*, The Combustion Institute, pages 847-864, Baltimore, 1953.

F.A. Williams, "Spray combustion and atomisation", *Phys. Fluids* 1 541-5, 1958.